2013

Fluidization of Nanoparticles: The Effect of Surface Characteristics

M. Tahmasebpoor
University of Tehran, Iran

Lilian de Martin
Delft University of Technology, Netherlands

M. Talebi
Delft University of Technology, Netherlands

N. Mostoufi
University of Tehran, Iran

J. R. van Ommen
Delft University of Technology, Netherlands

FLUIDIZATION OF NANAOPARTICLES: THE EFFECT OF SURFACE CHARACTERISTICS

M. Tahmasebpoor[a], Lilian de Martin[b] , M. Talebi[b] , N. Mostoufi[a] and J. R. van Ommen[b]*

[a] University of Tehran, School of Chemical Engineering
Tehran, Iran

[b] Delft University of Technology, Department of Chemical Engineering
2628 BL Delft, The Netherlands

*T: +31 15 2782133; F:+31 15 278 82 67; E: J.R.vanOmmen@tudelft.nl

ABSTRACT

An experimental study is conducted to determine the effect of surface properties of silica, alumina and titania nanoparticles on the fluidization characteristics of their agglomerates in a dry environment. The polar particles showed smaller bed expansion and larger minimum fluidization velocity compared to their apolar counterparts, indicating stronger inter-particle forces. The results show that part of the larger cohesion force observed between polar particles compared to apolar ones is due to direct hydrogen bridges between particles.

INTRODUCTION

In the last decade there has been a growing interest in nanoparticle fluidization as it can be an effective means for processing and handling of the ultrafine particles (1-4). The comparative studies on different types of nanoparticles have shown that some nanoparticles differ significantly from others in their fluidization behavior. Many researchers have categorized the fluidization behavior of the nanoparticle agglomerates into two types: agglomerate particulate fluidization (APF), group “A” like, and agglomerate bubbling fluidization (ABF), group “C” like behavior. The APF has been characterized by homogeneous bubbleless fluidization where agglomerates are observed to distribute uniformly throughout the bed. With increasing gas velocity, the fluidized bed expands consistently resulting in a high bed expansion ratio (1-2). The expanded bed exhibits fluid-like behavior (1). On the other hand, the ABF behavior is characterized by non-uniform fluidization with bubbles throughout the bed. The bed expands very little with increasing gas velocity, and large bubbles rise fast through the bed. The agglomerates are distributed nonuniformly within the bed: the large agglomerates move slowly at the bottom and the smaller agglomerates fluidize smoothly in the upper part (1,4). There is also a different approach to categorize nanopowder fluidization; solid-like to fluid-like to elutriation (SFE) behavior and solid-like to fluid-like to bubbling (SFB) behavior (5-6).

Based on primary particle size and material density, nanosized powders fall under the Geldart group C classification, which means that their fluidization is cumbersome because of cohesive forces (3). These forces (such as van der Waals, electrostatic, and capillary forces) will not let particles fluidize individually, but lead to the formation of agglomerates of several millions of particles and this large size of agglomerates hinders the fluidization (3,5). The van der Waals force between two equal smooth spherical particles of size d_p is

$$F_{vdW} = \frac{A_H d_p}{24 l^2} \quad (1)$$

where l is the minimum interparticle distance (~ 0.4 nm) and A_H is the Hamaker coefficient (7). If the surface of the nanoparticles has been coated with a material with different dielectric properties than the nanoparticles, the van der Waals force between the particles can be affected, influencing their agglomerate sizes, shapes, and fluidization behaviors. Yao et al. (1) and Liu et al. (3) showed that SiO_2 nanoparticles with surface modification of an organic compound achieve much higher bed expansions as compared with those that are not modified.

The second interparticle force expected in a fluidized bed is the electrostatic force. Electrostatics takes place when the charges inside a particle/agglomerate are displaced and then, the particle/agglomerate is polarized. Different authors minimize electrostatic effects by bubbling the gas through an alcohol–water solution before entering the bed. Electrostatic effects will be more important in non-conductive materials than in conductive ones. However, it is usually neglected when compared to the van der Waals interaction (1).

Capillary forces originate from adsorption and condensation of molecules on the particle surface forming liquid bridges between the particles. The surface tension of the liquid and the geometry of the formed neck influence the cohesion force. It is commonly accepted that in the presence of humidity capillary forces have an important contribution to the attraction between nanoparticles with an hydrophilic surface (1,8). However, the interaction between hydrophilic particles in dry environments is usually estimated with Eq. (1), using the Hamaker coefficient of the materials and ignoring the formation of direct hydrogen bonds (8).

Few experimental studies on nanoparticle fluidization include the effect of surface characteristics on hydrodynamic behavior such as U_{mf} and APF versus ABF behavior (1-3). In this paper we will consider several types of nanoparticles, both with a polar (P) and an apolar (A) surface. The objective of this study is to experimentally determine the influence of surface treatment of a variety of different nanoparticles with polar/apolar surface characteristics on their fluidization behavior in a gas-solid fluidized bed.

EXPERIMENTAL METHODS

The nanopowders were fluidized in a 26 mm i.d. glass column; the use of glass instead of the frequently used Perspex minimized the electrostatics. High-purity nitrogen was supplied to the bed through a porous plate distributor. To prevent the emission of nanoparticles to the atmosphere, the gas flow leaving the system is cleaned with a two-stage water bubbler and then filtered using a HEPA filter. The pressure drop across the bed was measured using a differential pressure transducer (Validyne Engineering, Model DP15-26) and recorded through the data acquisition system. The pressure drop across the bed was measured between two pressure taps. One of the pressure taps was located in the freeboard and the other 3.5 cm above the distributor.

Six different types of nanoparticles were investigated in this study: three different materials - silica, alumina and titania - and for each material a variant with an untreated surface (containing hydroxyl groups) and a surface with an organic

coating. These variants are described by the vendor as hydrophilic and hydrophobic. Since those terms are mainly used to describe the interaction of the materials with water and in this work there is no water present, we will stick to polar and apolar, respectively. The properties of particles are listed in Table 1. Before the experiments, the particles were sieved using a 335 µm sieve placed on a shaker.

The fluidization behavior of nanopowders was judged by the bed expansion and pressure drop. Also Fourier Transform Infra-Red (FTIR) spectroscopy was used for identification of organic compounds in the surface of nanoparticles.

Table 1 Properties of the primary particles used in this work

Powder	Material	Primary particle Size (nm)	Polarity	Bulk density (Kg/m^3)	Material density (Kg/m^3)
Aerosil 130	SiO_2	16	Polar	55	2200
Aerosil R972	SiO_2	16	Apolar	85	2200
Aeroxide Alu C	Al_2O_3	13	Polar	60	3600
Aeroxide Alu C 805	Al_2O_3	13	Apolar	85	3600
Aeroxide P 25	TiO_2	21	Polar	130	4000
Aeroxide T 805	TiO_2	21	Apolar	300	4000

RESULTS AND DISCUSSION

EFFECT OF INCREASING/DECREASING gas velocity

Pressure drop and bed expansion were measured as a function of gas velocity. These curves show a hysteresis when the gas velocity is increased from a packed bed to a fluidized bed (fluidization) or decreased from a fluidized bed to a packed bed (defluidization). Fig. 1 shows this for apolar silica, but the same was observed for all other particles. Previous studies attributed this hysteresis to contact or yield stresses and wall friction, which results in channeling or plugging of the nanoparticle agglomerates at low velocities (9-11).

Channeling of the nanoparticle agglomerates occurs at low velocities and gas prefers to pass through these channels by increasing the velocity until overcoming to cohesive forces between particles. We can see this phenomenon by some irregularities in the pressure drop and also by higher U_{mf} in the case of increasing in gas velocity owing to the irregular channel formation in the bed. The measured U_{mf} is more reproducible in descending gas velocity runs than ascending runs (12). Therefore, in this study, the characteristics of incipient fluidization were investigated by decreasing the superficial gas velocity in small steps (e.g., 0.5 mm/s). After each change in gas velocity, 5 minutes waiting time was taken for the bed to stabilize before the pressure drop was measured.

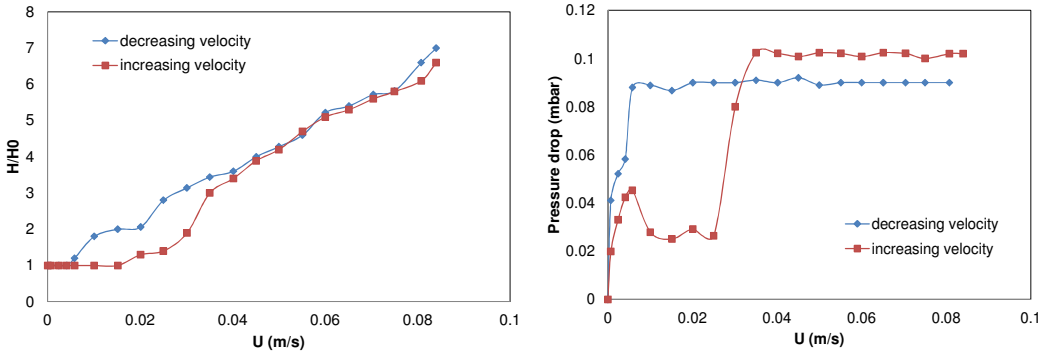

Figure 1 Bed expansion and pressure drop curves of SiO_2-apolar nanoparticles in decreasing and increasing runs

FLUIDIZATION BEHAVIOR: EFFECT OF SURFACE CHARACTERISTICS

The fluidization characteristics observed for different nanoparticles are summarized in Table 2. The fluidized bed of SiO_2 (A) particles behaved liquid-like as would be typically observed in the case of a Geldart group A powder in particulate (homogeneoous) fluidization. No bubbles were observed in the bed and very little carryover of the particles was observed until the gas velocity was sufficiently high. This kind of particle had thus APF behavior. All the other ones showed ABF behavior. For ABF particles, soon after the channels merged, the bed started to bubble and the bed behaved like a boiling liquid. Beyond minimum fluidization velocity, initially the pressure drop remained constant, but it soon started to decrease. This decrease in pressure drop was because of significant entrainment of particles from the bed which was further promoted by the vigorous bubbling of the bed.

Table 2 Summary of the fluidization behavior of different nanoparticles

Powder	Material	Fluidization type	U_{mf} cm/s	$H/H0$ at U_0= 5 cm/s
Aerosil 130	SiO_2 (P)	ABF	4	1.82
Aerosil R972	SiO_2 (A)	APF	0.6	4.28
Aeroxide Alu C	Al_2O_3 (P)	ABF	4	1.75
Aeroxide Alu C 805	Al_2O_3 (A)	ABF	2	2.55
Aeroxide P 25	TiO_2 (P)	ABF	5	1.60
Aeroxide T 805	TiO_2 (A)	ABF	4	1.72

The effect of the superficial gas velocity, U_0, on the fluidized bed height for all particles has been presented in Fig. 2. As shown, for all three kind nanoparticles, polar particles achieve lower bed than apolar particles. This difference is largest for SiO_2 particles. Usually, the polar particles showed a tendency to stick to the wall or there was observed a layer of large sized agglomerates slowly moving at the bottom of the bed. Besides, for lower gas velocities, the channels formed in the bed of polar particles were very stable as compared to that of the apolar particles. As a result, the gas velocity at which the channels were merged was higher for the polar particles. Consequently, the minimum fluidization velocity for polar particles was higher than that of the apolar particles (see Table 2). This was also found by Zhu et al. (2).

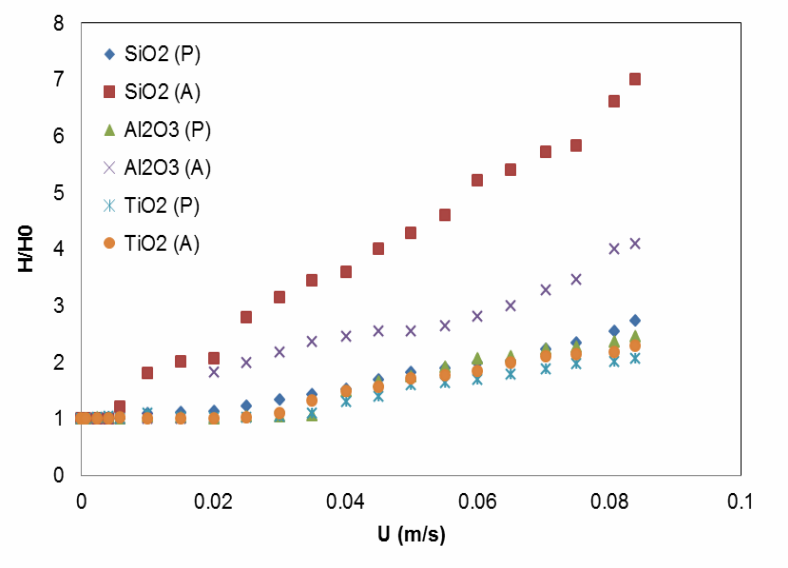

Figure 2 Bed expansion curves of all nanoparticles

As mentioned before, the fluidization of apolar nanoparticles is smoother than that of polar nanoparticles. This observation can be attributed to the presence of active hydroxyl groups on the surface of the polar particles. These exposed hydroxyl groups are able to form hydrogen bridge linkages with the hydroxyl groups of other polar particles, increasing the interaction between the particles (13). In order to improve the functionality and dispersibility of the particles, vendors also offer particles with a treated surface: most of the hydroxyl groups are replaced with suitable organic groups as illustrated in Fig. 3 (14). This process is called the 'hydrophobization process' as it imparts water repellent properties to the original polar particles. Hydrophobization gives the apolar particles distinctly better dispersibility than the polar particles by replacing strong attractive forces, resulting from the stable hydrogen bridges, with the much weaker van der Waals dispersive forces as depicted in Fig. 3 (14-15).

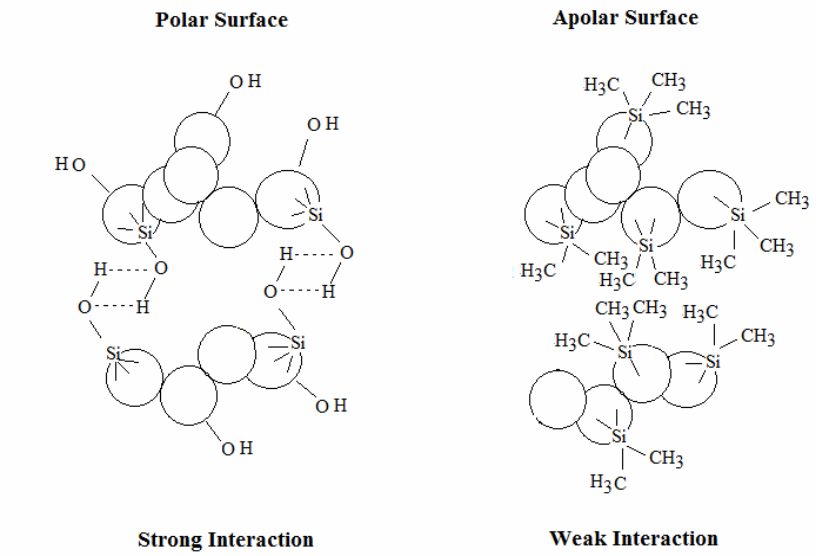

Figure 3 Comparison of particle-particle interactions for particles with polar and apolar surfaces.

FTIR data at 3700–700 cm^{-1} for polar and apolar particles are shown in Fig. 4. These curves confirm the above mentioned discussion about effect of surface treatments. Circles show the absorption at bands near the stretching vibration of the hydrocarbon groups (13, 16-18), which can be attributed to the surface treatments of apolar ones. No peak was observed for the polar particles above this wave number range using the FTIR analysis but this absorption band was observed for apolar particles. These results clearly show that in the apolar particles active surface groups are replaced by means of surface treatments.

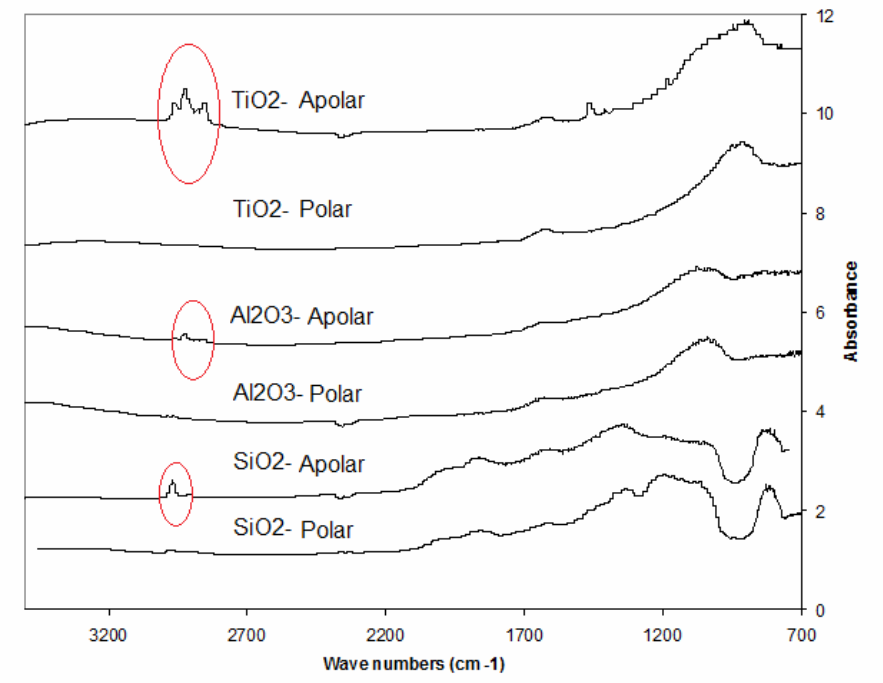

Figure 4 FTIR absorption spectra of the used nanoparticles Circles show the absorption at bands near the stretching vibration of hydrocarbon groups (13, 16-18)

A simple calculation of the energy of cohesion between nanoparticles is shown in Table 3. The van der Waals interaction potential U_{vdW} between two smooth spheres separated a distance *l* is

$$U_{vdW} = -\frac{A_H d_p}{24l} \tag{2}$$

The energy of the hydrogen bond formed between the polar particles is strong which keeps the particles together. The apolar nanoparticles have hydrocarbon groups on the surface (16-18) giving weaker interaction, so the inter-particle forces will be dominated by the contribution of the material of the cores. For the apolar nanoparticles, the bed expansion decreases in the order SiO_2 -Al_2O_3 - TiO_2. This can be attributed to differences in the density of the nanoparticles as well as in the Hamaker coefficient of the core material (19). The SiO_2 (A) presents the highest bed expansion compared with the other apolar nanoparticles, which is in agreement with the lowest particle density and lowest Hamaker coefficient. The TiO_2 (A) presents the lowest bed expansion, explained by their highest particle density and a large Hamaker coefficient (see Table 3).

The results show that the bed expansion is very different for the apolar particles ($2 < H/H_0 < 7$) but similar for all the polar particles ($H/H_0 \sim 2$). This indicates that all the polar nanoparticles are dominated by the same force due to the hydrogen bridges. The bed expansion is independent of the Hamaker coefficient of the core material and the particle density. Contrary, the bed expansion of the apolar nanoparticles is strongly influenced by the Hamaker constant of the core material and the particle density. The same conclusion can be drawn looking at the minimum fluidization velocities (Table 2). U_{mf} for the apolar particle ranges from 0.6 to 4 cm/s whereas the range for the polar ones is much narrower, from 4 to 5 cm/s.

These calculations also explain why polar and apolar SiO_2 nanoparticles present the largest difference in the fluidization behavior. Due to the low Hamaker coefficient and small particle size of the SiO_2 nanoparticles, the van der Waals potential between them is so low that the formation of only a few hydrogen bridges between them already provides a similar potential. On the other extreme, TiO_2 nanoparticles show a minimum fluidization velocity and a bed expansion hardly affected by the presence of the hydrogen bonds. The Van der Waals force between TiO_2 particles is already large – both Hamaker constant and particle size are relatively large – so the formation of a few hydrogen bonds does not make an appreciable difference; see Tamhasebpoor et al. [20] for a more detailed discussion.

Table 3 Estimation of the influence of the surface groups on the total interaction between different nanoparticles. P and A represent polar and apolar surfaces. The interparticle distance to estimate the interaction potential is 0.4 nm in all the cases.

Core Material	**Interaction dominating the shortest scales**	**A_H of the core material (J) * (19)**	**Interaction potential U_{vdW} (J)**
SiO_2 (P)	OH···H ~3×10^{-20} J/bond	6.60×10^{-20}	~1×10^{-19}
Al_2O_3 (P)		1.45×10^{-19}	~2×10^{-19}
TiO_2 (P)		1.54×10^{-19}	~3×10^{-19}
SiO_2 (A)	Organic group <<10^{-20} J/bond	6.60×10^{-20}	~1×10^{-19}
Al_2O_3 (A)		1.45×10^{-19}	~2×10^{-19}
TiO_2 (A)		1.54×10^{-19}	~3×10^{-19}

* Hamaker coefficient measured in vacuum taking into account retardation

CONCLUSIONS

Polar particles have smaller bed expansion and higher U_{mf} than apolar particles. This is because of stronger interparticle forces in case of polar particles, caused by the presence of hydroxyl groups that form hydrogen bonds between particles. The apolar nanoparticles have organic groups on the surface and the inter-particle forces are dominated by the contribution of van der Waals forces.

All polar nanoparticles have similar bed expansions and U_{mf} due to the strength of the hydrogen bond between the particles. The van der Waals forces between the apolar particles are strongly influenced by the material of the cores. As a result, apolar SiO_2 has the highest bed expansion (lowest U_{mf}) and apolar TiO_2 (A) has the lowest bed expansion (highest U_{mf}) which is in agreement with corresponding Hamaker constant and the particle density.

REFRENCES

1- W. Yao, G. Guangsheng, W. Fei and W. Jun, Pow. Tech., 124:152, 2002.
2- C. Zhu, Q. Yu, R. N. Dave and R. Pfeffer, AIChE J., 51:426, 2005.
3- H. Liu, Q. Guo and S. Chen, Ind. Eng. Chem. Res., 46:1345, 2007.
4- X.S.Wang, F. Rahman and M.J. Rhodes, Chem. Eng. Sci., 62:3455, 2007.
5- J. M. Valverde and A. Castellanos, Chem. Eng. Sci., 62:6947, 2007.
6- J.R. van Ommen, J.M. Valverde and R. Pfeffer, J. Nanopart. Res., 14:737, 2012.
7- K. Rietema, K. The Dynamics of Fine Powders. Elsevier, London, 1991.
8- J. M. Valverde and A. Castellanos, Chem. Eng. J., 140:296, 2008.
9- P.N. Loezos, P. Costamgna and S. Sundaresan, Chem. Eng. Sci., 57:5123, 2002.
10- S.C. Tsinontides and R. Jackson, J. Fluid. Mech., 225:237, 1993.
11- X. Liu, G. Xu and S. Gao, Chem. Eng. J., 137:302, 2008.
12- C. L. Lin, M. Y. Wey, S. D. You, Powder. Tech., 126:297, 2002.
13- Degussa AG, Technical Bulletin Fine Particles No. 11, Basic Characteristics of AEROSIL® Fumed Silica.
14- M. Scholz and M. Kempf, Technical Bulletin Pigments, No. 12, Degussa AG technical report, 2001.
15- F. Rahman, Fluidization Characteristics of Nanoparticle Agglomerates, Department of Chemical Engineering, Ph.D. Thesis, Monash University, 2009.
16- P. Larkin, Infrared and Raman Spectroscopy; Principles and Spectral Interpretation, Elsevier Science Ltd, 2011.
17- C. Schilde, H. Nolte, C. Arlt and A. Kwade, Compos. Sci. Technol., 70:657, 2010.
18- B. Erdem, R. A. Hunsicker, G. W. Simmons, E. D. Sudol, V. L. Dimonie and M. S. El-Aasser, Langmuir, 17:2664, 2001.
19- H. D. Ackler, R. H. French and Y.-M. Chiang, J. Colloid Interface Sci., 179:460, 1996.
20- M. Tahmasebpoor, L. de Martín, M. Talebi, N. Mostoufi and J. R. van Ommen, Phys. Chem. Chem. Phys., DOI: 10.1039/C3CP43687J, in press, 2013.